International Journal of Plasticity 38 (2012) 1–13

Contents lists available at SciVerse ScienceDirect

International Journal of Plasticity

journal homepage: www.elsevier.com/locate/ijplas

Deformation induced anisotropic responses of Ti–6Al–4V alloy. Part I: Experiments

Akhtar S. Khan, Shaojuan Yu *

Department of Mechanical Engineering, University of Maryland, Baltimore County, 1000 Hilltop Circle, Baltimore, MD 21250, USA

ARTICLE INFO

Article history:
Received 5 October 2011
Received in final revised form 21 February 2012
Available online 4 April 2012

Keywords:
Titanium alloy
Anisotropy
Tension compression asymmetry
Strain rate and temperature dependent
Confining pressure

ABSTRACT

The anisotropic thermo-mechanical behaviors of an electron beam single melt Ti–6Al–4V alloy over a wide range of strain rates from quasi-static to dynamic regimes, and at various temperatures from 233 to 755 K, are reported. The anisotropic responses are determined along different directions (the rolling, the transverse-to-rolling and the thickness directions). Measured responses are presented along these directions during uniaxial compression and tension loadings. Results are also given for behaviors under low confining pressures. Along with positive strain rate sensitivity and negative temperature dependency, the responses along the thickness and transverse to rolling direction are found to be close to each other. Along the rolling direction, it is much higher than the other two directions. The equivalent stress–strain curves are found to be independent of the confining pressure. The Khan–Huang–Liang (KHL) phenomenological model is used to predict the observed anisotropic thermo mechanical behaviors. A systematic method is employed to determine the model material constants utilizing the experimental data. By using the calibrated material constants, the capability of the constitutive model to predict thermo mechanical response of the alloy is evaluated by comparison of the numerical simulations and experimental observations. It is found that there is a close agreement between the simulated results and the experimental observations.

1. Introduction

The titanium and its alloys have attracted more and more interests from aerospace, energy and chemical processing industries since their emergence in the early 1950s. They have higher mechanical strength to weight ratio but are 40% lighter than steel (Nixon et al., 2010). The excellent high strength to weight ratio as well as the capability to withstand high temperature make them an excellent candidate for the material used on aero-engines, gas turbines and aero-space structures where light-weight and heat resistance are desired. The excellent physical–mechanical properties of these materials, such as good resistance to corrosion and biocompatibility, keep finding new area of utilizations for this metallic system in medical and petrochemical industries (Gilat and Cheng, 2002; Khan et al., 2004; Bjerke et al., 2002). Dynamic responses of metals have been of interest not only in impact and penetration related problems (Khan et al., 2004, 2012; Khan and Baig, 2011) but also in high speed machining (Molinari et al., 2002). The development of relatively economical Ti–6Al–4V alloy, with resulting high oxygen content, has sparked interest in its possible use in lightweight tanks (Montgomery and Wells, 2001; Nemat-Nasser et al., 2001); the conventional, more expensive Ti–6Al–4V alloy has been used primarily in aerospace components. The potential applications in armor, including ceramic tiles encapsulated in titanium alloys, have motivated several studies (Lesuer, 2000; Nemat-Nasser et al., 2001; Majorell et al., 2002).

* Corresponding author.
E-mail addresses: khan@umbc.edu (A.S. Khan), syu1@umbc.edu (S. Yu).

0749-6419/$ - see front matter © 2012 Elsevier Ltd. All rights reserved.
http://dx.doi.org/10.1016/j.ijplas.2012.03.015

In case of α-titanium, it has been demonstrated that the deformation mechanisms include glide systems with α-type dislocations in the HCP structure, as well as twinning shear which contributed to the overall strain (Meyers et al., 1994; Song and Gray, 1995; Chichili et al., 1998). In the quantitative study of twinning, Chichili et al. (1998) have shown that twin density increases drastically with increase in strain rate. The rate of increase of this density decreased with increase in strain at dynamic strain-rates of $10^3\ s^{-1}$, while this rate increased with deformation in the case of quasi-static loading ($10^{-5}\ s^{-1}$). Their results further demonstrated that loading at a particular temperature (and/or strain rate), unloading, and reloading at another temperature (and/or strain rate), resulted in a stress–strain curve which was significantly different, if the specimen was loaded at the latter temperature (and/or strain rate) right from the beginning. Their study was performed over a wide range of strain rates (10^{-5}–$10^3\ s^{-1}$), but over a very limited range of temperatures (77–298 K).

The Ti–6Al–4V alloy consists of HCP α-grains, with a dispersion of stabilized BCC β phase around grain boundaries at room temperature. α phase transforms to β phase starting at 873 K; above 1268 K, the entire microstructure consists of equiaxed β phase (Majorell et al., 2002). This alloy, in addition to H, V, and Ti, contains O, Fe, Mo, C, Si, and Mn. Oxygen, nitrogen, and carbon contents are α stabilizers (Conrad et al., 1973), while vanadium, iron and molybdenum are β stabilizers. Conrad et al. (1973) proposed equivalent oxygen content ($O_{eq} = O + 2N + 0.75C$); this equivalent impurity concentration gives the effect of dislocations-impurity interaction on the yield strength of the material. Investigation by Majorell et al. (2002) was on an untextured and a textured Ti–6Al–4V alloy rod that was manufactured by Allvac. This study was over a strain-rate range of 10^{-3}–$10\ s^{-1}$ and a temperature range of 650–1345 K. They did not observe any dynamic strain-aging at any of the investigated temperatures or strain rates. Further, athermal stress, i.e., temperature insensitive response, was found at approximately 1255 K; i.e. at a temperature when the material contained almost 100% β phase. The equivalent oxygen content was 0.206%.

In a study by Follansbee and Gray (1989) on a Ti–6Al–4V alloy, with an equivalent oxygen content of 0.23% (actual oxygen was 0.18%), the measurements were restricted to three temperatures ranging between 76 and 295 K, and at only two strain rates (10^{-3} and approx. $3000\ s^{-1}$). Their specimens on as-received and two heat-treated conditions were made from a 13.8 mm thick plate. This investigation did not include responses over a wide range of temperatures. The Nemat-Nasser et al.'s (2001) study was on a commercial and two hot isostatically pressed Ti–6Al–4V alloys. The equivalent oxygen in the commercially pure alloy was 0.22%. They performed experiments on specimens at temperatures ranging from 77 to 998 K at the dynamic strain rate regime of 2000–4000 s^{-1}. As discussed, α-phase starts transforming to β-phase at 873 K. Thus, they performed experiments on presumably different materials in their range of temperatures; i.e., with different amounts of α and β phases. They suggested that all (i.e., 100%) of plastic work done was converted to heat. This conclusion is in direct contradiction with the measurements of Macdougall and Harding (1999), and Rosakis et al. (2000).

The constitutive models used for high strain rate applications can be classified in two categories; the purely phenomenological ones; e.g., the ones by Johnson and Cook (1983), Sung et al. (2010), Steglich et al. (2011), and Khan–Huang–Liang (KHL) models (Huang and Khan, 1991; Khan and Liang, 1999; Khan et al., 2004, 2012; Khan and Baig, 2011), *etc.*, and so called, "physically based models"; e.g., the ones by Zerilli and Armstrong (1987), Mecking and Kocks (1981), *etc.*, that were used by Follansbee and Gray (1989), and in a modified form by Nemat-Nasser et al. (2001). The latter group discusses the mechanisms of plastic deformation (mainly dislocations). However, the material constants are determined by not measuring any deformation mechanism related quantity, but by choosing constants to "fit" the uniaxial stress–strain curves at different strain rates and temperatures; similar to those purely phenomenological models. In the simplification or modification of the model by Nemat-Nasser et al. (2001), experiments are needed at very high temperatures where proper lubrication is extremely difficult, if not impossible, to attain. Since in both categories of models, phenomenological and so called "physically based", material constants are determined by "fitting" to the stress–strain responses at different temperatures and strain rates, the advantage of one over the other is primarily the number of material constants in each model. Any model with a large number of material constants will be able to approximate the observed responses. Mecking and Kocks model, as used by Follansbee and Gray (1989) has 23 constants, while these constants are ranging from 12 to 8 in case of Cheng and Nemat-Nasser (2000) and Nemat-Nasser et al. (2001) respectively, depending on whether they include modeling of dynamic strain aging or not. Johnson–Cook (J–C) and Khan–Huang–Liang (KHL) models have 5 and 6 constants, respectively. Johnson–Cook and Khan–Huang–Liang models are used in this investigation due to their advantage of fewer constants and their ability to model the observed material response as closely as those with many more constants. Also, Khan et al. (2004) have shown that the KHL model has more flexibility than J–C model, and can accurately describe the observed responses in Ti–6Al–4V ELI and other titanium alloys.

The main objective of this research is to investigate anisotropic deformations of the Ti–6Al–4V alloy at different strain rates, temperatures, and superimposed hydrostatic pressures. In this comprehensive study, the responses of the alloy were determined in three directions (to study anisotropy), at low to high temperatures (to determine temperature effect), at low to high strain rates (to quantify strain rate dependency), under tension and compression to investigate asymmetry in tension–compression, and compression response under changing the hydrostatic pressure at different strain rates. Then some of the measured responses are modeled using the KHL constitutive equation.

2. Experiment details

An electron beam single melt Ti–6Al–4V alloy, with an equivalent oxygen content ($O_{eq} = O + 2N + 0.75C$) of 0.222%, was used in this study. All the specimens were machined from the same rolled plate with a thickness of 25.4 mm. The specimens

were loaded under different nominal strain rates and along loading axes of the rolling direction (RD), transverse-to-rolling direction (TD) and the thickness direction (ND).

2.1. Uniaxial compression

All compression experiments were performed in as-received condition, at different strain rates ranging from 10^{-4} to $10^{3}\ s^{-1}$, and at different temperatures ranging from 233 to 755 K.

Quasi-static uniaxial compression loading experiments, ranging from 10^{-4} to $1\ s^{-1}$, were conducted using a MTS axial/torsional servo-hydraulic 809 system. In the case of compression, Teflon sheets and Dow Corning high vacuum grease were applied at the cylindrical specimen ends to reduce friction and to maintain uniform uniaxial stress state. High elongation uniaxial strain gage (KFEL-2-120-C1 manufactured by Kyowa Ltd. (Japan)) was used to measure strains at room temperature during these experiments; gage factor and bridge non-linearity corrections were applied to recorded strains (Huang and Khan, 1991). High and low temperature chambers were used to investigate the temperature dependency of the Ti–6Al–4V alloy. For compression experiments, the diameters of the cylindrical specimens were 7.92 mm with a length to diameter ratio of 1.5.

The mechanical response of the material under dynamic loading was determined by using compressive Split-Hopkinson Pressure Bar (SHPB) technique. The SHPB pressure bars were made from Vascomax C-350 steel with diameters of 12.7 mm. Disc samples were machined with a gage length to diameter ratio of 0.5 (7.92 mm in diameter) with axes lined up with one of the anisotropy directions. In order to obtain the dynamic response of the alloy at elevated temperatures, the specimen was heated to a desired temperature level. Dow Corning high temperature grease was applied the interfaces between the sample and the bars to reduce the friction. The incident and transmitted bar ends, next to the specimen were cooled to avoid heating of these bars.

Isothermal condition existed when the strain rate was lower than $10^{0}\ s^{-1}$. For the experiments with strain rate of $10^{0}\ s^{-1}$, the loading-unloading-reloading procedure proposed by Khan et al. (2007a) was adopted. The specimen was unloaded for each 5% strain increment and allowed to cool at room temperature for 30 min before reloading. It was then reloaded to the next 5% of strain. The stress–strain curves shown are the envelope of starting plastic deformation in each reloading part before thermal softening started again. Then correlations with the KHL model is done for the isothermal case. The temperature increase of the material subjected to adiabatic (dynamic) loading condition was determined by the following equation, where β (the value of 0.9 was used for current material) was the fraction of plastic work converted to heat, ρ and C_p were the mass density and the specific heat at constant pressure for the material, respectively. A detailed description of the evaluation of the temperature rise in a similar material can be found in another paper (Khan et al., 2004). The correlations from KHL model were adjusted for this temperature rise and then compared with adiabatic experimental results

$$\Delta T = \frac{\beta}{\rho C_p}\int_0^{\varepsilon}\sigma(\varepsilon)\mathrm{d}\varepsilon$$

More details of the SHPB technique and the associated calculations can also be found in Follansbee and Gray (1989) and Khan and Zhang (2000).

2.2. Uniaxial compression under superimposed hydrostatic pressure

It has been found that the flow stress of metals is influenced by pressure (e.g. Brownrigg et al., 1983; Spitzig and Richmond, 1984; Kao et al., 1989). In this research, uniaxial compression experiments were performed in a specially designed pressure vessel, as shown in Fig. 1. The pressure vessel was installed between the upper and lower grips of the MTS 809 testing system to conduct these compression experiments. The cylindrical specimens for compression experiments with superimposed hydrostatic pressure had diameters of 7.92 mm with a length to diameter ratio of 1.5. Experiments were performed in as-received condition.

Before conducting the experiment, the specimen was carefully aligned inside the pressure vessel so that its axis was coincident with that of the loading bar. The interfaces between the specimen and loading grips were lubricated by a layer of Teflon tape and grease. Then, the pressure vessel was aligned on the MTS 809 material testing machine. A three-step-loading path was used during the experiment to investigate the mechanical responses of the alloy under superimposed hydrostatic pressure. In the first step, pressured fluid was slowly injected from the bottom of the vessel by the pressure intensifier with a relief opening at the top of the vessel in open position to get rid of the air in the vessel. Then this hole was closed and pressure was allowed to increase to a desired constant hydrostatic pressure. During this step, the loading bar was kept stationary by the MTS machine. A significant increase in load was measured by the MTS machine (load cell) which was due to the pressure added on the bottom end of the loading bar. In the final step, axial loading at a constant strain rate was imposed on the specimen at the desired level of superimposed hydrostatic pressure. The axial load consisted of two parts, a negative load due to pressure on the annular area (cross-section difference between the specimen and loading fixture) and a positive load applied through the MTS system.

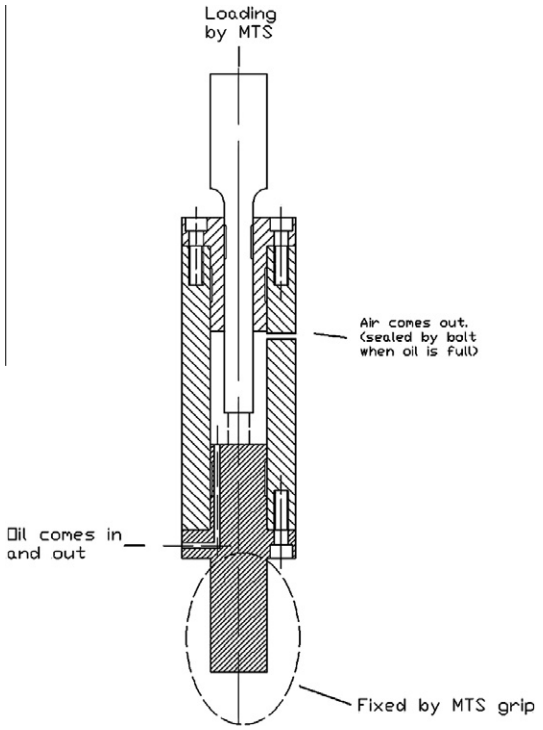

Fig. 1. A schematic drawing of the pressure vessel and loading grips.

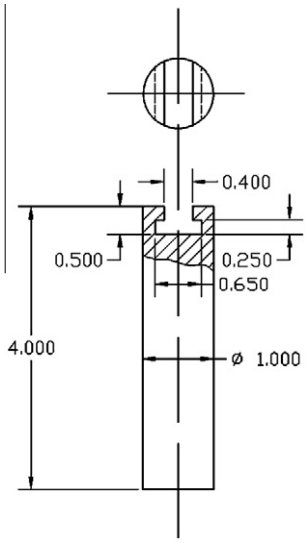

Fig. 2. A schematic drawing of the tension loading grips.

2.3. Uniaxial tension

To conduct uniaxial tension experiments on MTS 809 material testing machine, special loading grips were designed, as shown in Fig. 2. During the test, one end of the loading grip was inserted into the loading grip of MTS machine. The other end of the grip had a T-shaped groove which could fit the holding portion of the specimen. Prior to the experiment, the T-shaped grooves of the two tensile loading grips were set to make a 90° angle. This helped to align the specimen in the center of the grips and prevented the specimen from sliding out during the experiment. Smooth round bar tensile specimen was used in the present research. Fig. 3 shows the geometry of the tensile specimen. The maximum dimension of the specimen

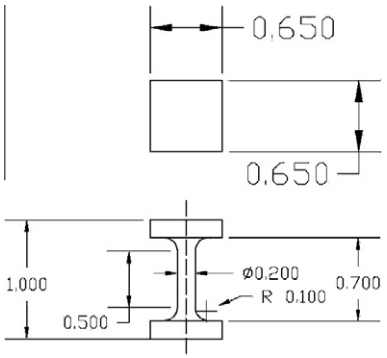

Fig. 3. The geometry of the tension specimen.

which was along axial loading direction was limited by the smallest dimension of the rolled plate which was 25.4 mm along the thickness direction. Experiments were performed in as-received condition

The axial loading directions of the machined specimens were along RD, TD, and ND. These specimens were loaded at different strain rates, ranging from 10^{-4} to 1 s^{-1}. For each strain rate, a series of experiments were performed at different temperatures ranging from 233 to 755 K. A thermocouple was mounted directly on the surface of each specimen to accurately monitor the temperature during the experiment. The strain in the specimen was calculated by using the MTS displacement transducer output which was corrected for elastic deformation of the load train.

3. Experimental results

3.1. Anisotropic responses of the material at room temperature

At room temperature, the mechanical responses of the alloy under uniaxial compressive loading were characterized along three material principal directions of the alloy plate (rolling, transverse-to-rolling as well as thickness direction). In Fig. 4, true stress–true strain relations along the three principal directions are presented at different strain rate ranging from 10^{-4} s^{-1} to dynamic strain rate and at room temperature. As seen in Fig. 4, the mechanical behavior of the alloy along each direction is highly strain rate sensitive. The yield and flow stresses show a positive dependency on the strain rate, while a slight negative dependency of work hardening rate on strain rate was observed on quasi-static region and becomes more obvious in dynamic region due to thermal softening which is caused by the heat generated during plastic work. Comparing all the three principal loading directions, the response in the rolling direction is much higher than the ones in transverse and thickness directions; the responses are almost identical in the two latter directions. Further, a strong strain rate effect is visible in this figure. In order to follow responses in a particular direction, a different color is used for each direction. The strain rate effect varies nonlinearly with increase in the strain rate.

3.2. Temperature dependent anisotropic responses

To examine the temperature effect on the mechanical behavior of the Ti–6Al–4V alloy along three principal material directions, three set of uniaxial compression experiments were performed at various temperature ranging from 233 to 755 K, and at constant strain rates.

Fig. 5 contains responses along the rolling (RD), transverse (TD) and thickness, or normal (ND) directions at different temperatures, at a strain rate of 10^{-3} s^{-1}. The temperatures were 233, 296, 422, 589 and 755 K. Again, the response in each direction is shown by a different color. The anisotropy is observed to depend non-linearly on the temperature; this dependency is stronger than the strain rate effect illustrated in the earlier figures. An inverse temperature dependence of the mechanical strength of the alloy along the rolling direction was observed when the material was subjected to different temperatures. Throughout the examined temperature range, it can be clearly found that the yield stress, flow stress level as well as the work hardening rate decrease continually with the increase of temperature due to the thermal softening effect. Again, similar thermo-mechanical responses of the alloy along transverse-to-rolling and thickness direction were observed.

The measured anisotropic responses at high strain rates are shown in Figs. 6 and 7. The strain rates shown in these figures, increase from approximately 1000 to around 3000 s^{-1}. These dynamic responses were measured using compression SHPB technique at low and high temperatures. These responses are very non-linearly dependent on strain rate and temperature.

The metallic materials with different crystal structure, such as F.C.C. (face-centered cubic) structure, B.C.C. (body-centered cubic) structure, and H.C.P. (hexagon-close packed) structure, show distinct different dependency of mechanical responses on strain rate and temperature. In F.C.C. materials, during plastic deformation, the dominant resistance to the glide of activated dislocation is resulted from the energy barriers of forest dislocations. Thus, at a specific temperature range, the initial yield and flow stresses of F.C.C. materials are insensitive to the change of strain rate (Nemat-Nasser and Li, 1998).

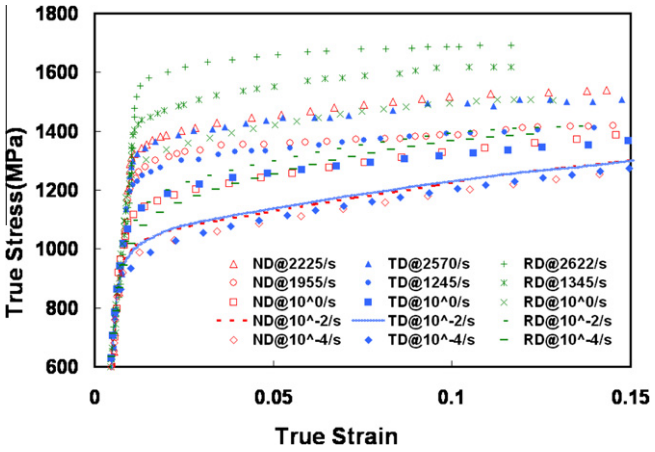

Fig. 4. Anisotropic responses under compression in three directions at 296 K, and at different strain rates in quasi-static and dynamic regimes.

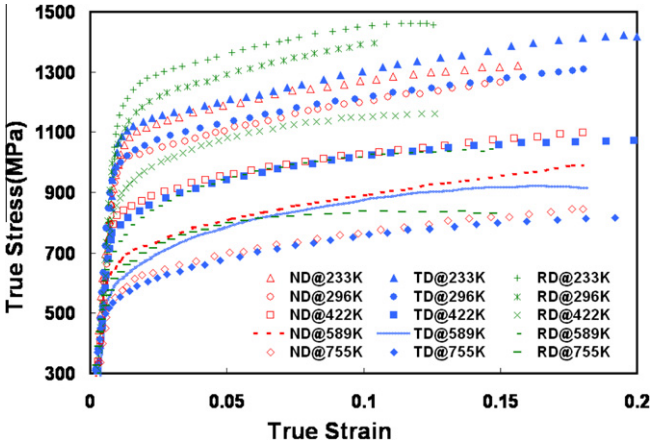

Fig. 5. Temperature dependent anisotropic responses under compression in three directions, at a constant strain rate of 10^{-3} s^{-1}.

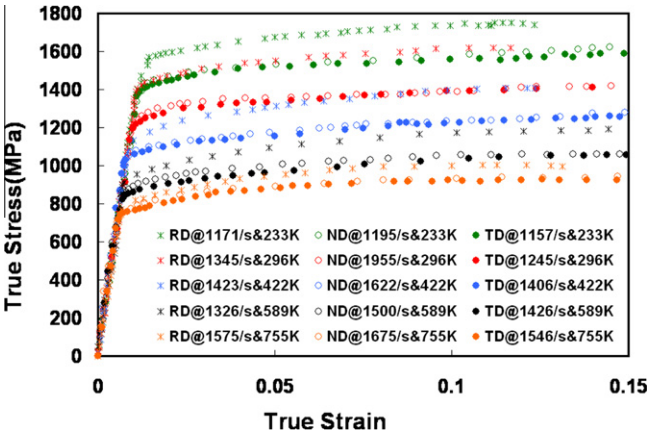

Fig. 6. Different anisotropic responses in dynamic compression (at strain rates from 1157 to 1955 s^{-1}), in three directions; measured results at 233, 296, 422, 598 and 755 K are shown using green, red, blue, black and orange symbols, respectively. (For interpretation of the references to color in this figure legend, the reader is referred to the web version of this article.)

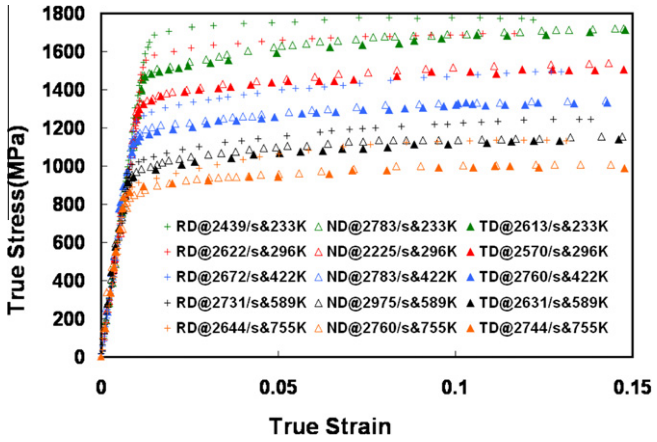

Fig. 7. Different anisotropic responses in dynamic compression (at strain rates from 2225 to 2975 s^{-1}), in three directions; measured results at 233, 296, 422, 598 & 755 K are shown using green, red, blue, black and orange symbols, respectively. (For interpretation of the references to color in this figure legend, the reader is referred to the web version of this article.)

Whereas, in B.C.C. and H.C.P. materials, the dominant energy barrier to the thermal activation of mobile dislocations is resulted from the interaction between the activated dislocation and the crystal lattice, which is referred to as Peierls-Nabarro barriers (Hoge and Mukhejee, 1977; Peirce et al., 1983). Therefore, the thermo-mechanical behaviors of B.C.C. and H.C.P. materials show strong strain rate and temperature dependencies. The increase of strain rate leads in elevating the yield and flow stresses to higher stress levels. In B.C.C. and H.C.P. materials, the activation volume (or area), which is defined as the separation distance between points of dislocation obstacles, is not altered when the deformation proceeds at a constant strain rate or temperature. While in F.C.C. material, the activation volume keeps decreasing with the increase of plastic strain due to the multiplication of both activated and forest dislocations (Nemat-Nasser et al., 1998). Therefore, in B.C.C. and H.C.P. materials, the increasing of strain rate only translates the stress strain curve to a higher level but does not change the curvature of the strain hardening curve (Armstrong et al., 1988). Comparing with the dependence of strain rate, it can be clearly found that the mechanical behavior of the material has more pronounced temperature sensitivity. This result is consistent with those presented by Nemat-Nasser et al. (2001). The observed decrease of the strain hardening rate of the material in dynamic region can be also attributed to the negative temperature effect on the mechanical response of the alloy.

3.3. Tension–compression asymmetry

The behavior of the alloy is significantly different in tension and compression as shown in Fig. 8. There is an appreciable difference not only in yield stress levels but also in work hardening. The anisotropic responses in tension and compression are shown at the room temperature at strain rates in quasi-static loading regime. The failure strains in tension are slightly lower than in compression; the failure strains in thickness direction (ND) in compression loading are much higher than rolling direction (RD), while failure strains in the transverse to rolling direction (TD) are in between the other two directions.

3.4. Material responses under superimposed hydrostatic pressure

In Fig. 9, the responses of the alloy under superimposed hydrostatic pressure are shown at different superimposed hydrostatic pressures and four different strain rates in the rolling direction. These experiments were performed with the specimens loaded in compression inside a pressure vessel, thus the cylindrical surface of the specimens were subjected to a superimposed hydrostatic or confining pressure. The pressure inside the pressure chamber was changed to get different superimposed hydrostatic pressures. The stress–strain curves appear to shift by the amount of superimposed hydrostatic pressure. These measured responses are re-plotted in terms of von Mises equivalent stress and strain in Fig. 10, there is almost negligible effect of the superimposed hydrostatic pressure at these low hydrostatic pressures. Similar measured responses in TD and ND directions are shown in Figs. 11 and 13, respectively in terms of stress and strain; Figs. 12 and 14 contain the same measured responses in terms of von Mises equivalent stress and strain.

4. Constitutive model

4.1. Khan–Huang–Liang (KHL) constitutive model

In this research, the Khan–Huang–Liang (KHL) constitutive model is used to simulate the anisotropic mechanical responses of the alloy. The following equation shows the KHL plastic constitutive model which has been used to successfully predict the isotropic thermo mechanical behavior of different materials (Khan and Liang, 1999; Khan et al., 2004, 2007, in press).

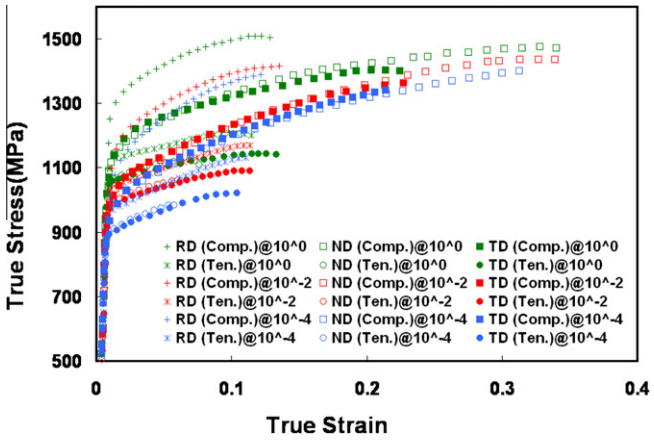

Fig. 8. Different anisotropic responses in tension and compression, in three directions at 296 K; experimental results at a strain rate of 10^{0}, 10^{-2} and 10^{-4} s^{-1}, are shown in green, red and blue colors. (For interpretation of the references to color in this figure legend, the reader is referred to the web version of this article.)

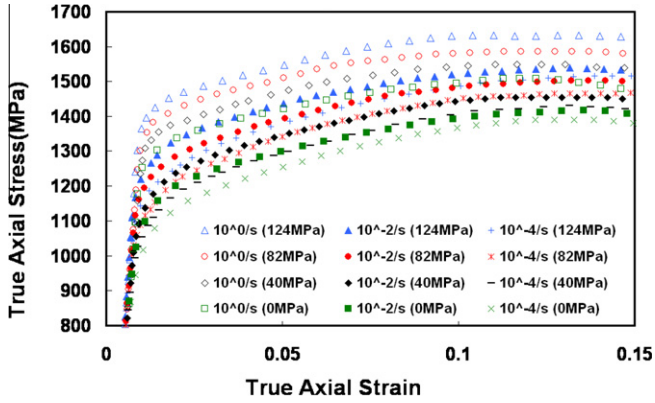

Fig. 9. Measured responses in compression along rolling direction (RD), under different superimposed hydrostatic pressures ranging from 0 to 124 MPa.

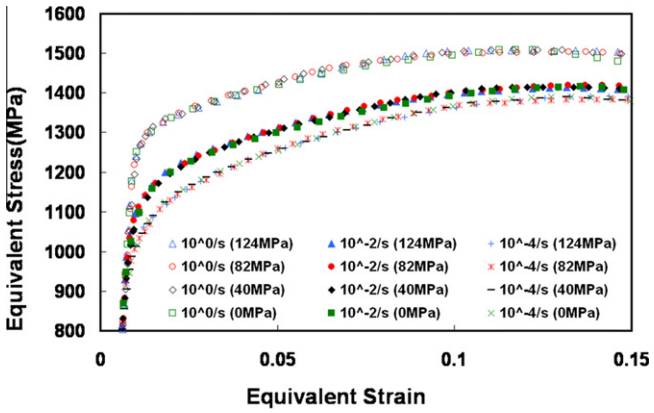

Fig. 10. Responses in compression along rolling direction (RD), under different superimposed hydrostatic pressures ranging from 0 to 124 MPa, in terms of equivalent stresses and strains.

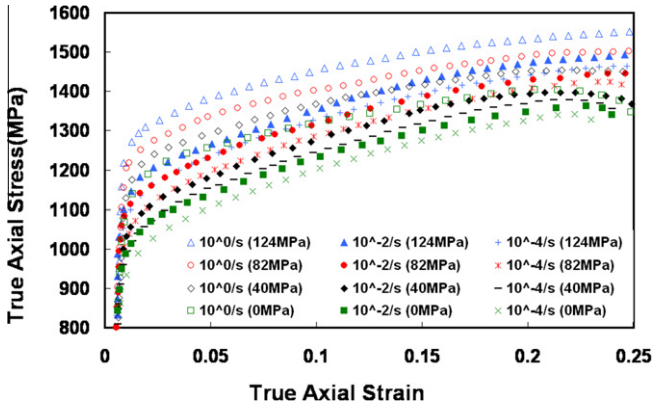

Fig. 11. Measured responses in compression along transverse to rolling direction (TD), under different superimposed hydrostatic pressures ranging from 0 to 124 MPa.

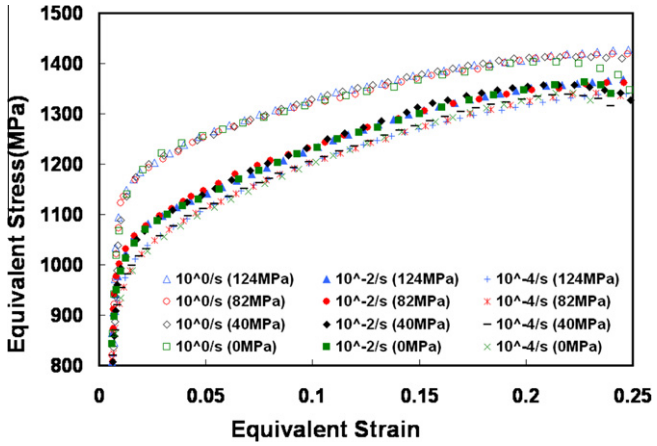

Fig. 12. Responses in compression along transverse to rolling direction (TD), under different superimposed hydrostatic pressures from 0 to 124 MPa, in terms of equivalent stresses and strains.

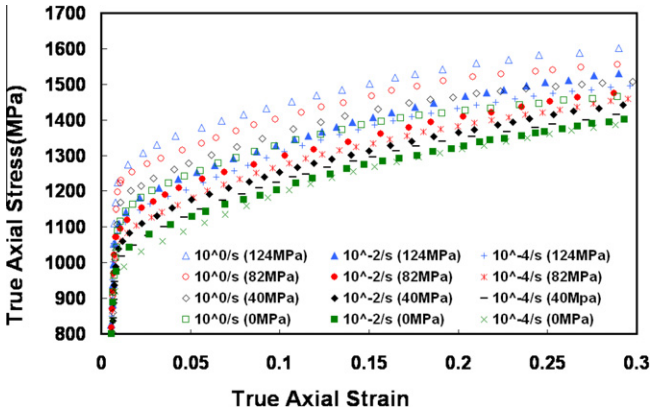

Fig. 13. Measured responses in compression along normal to rolling plane (ND), or through thickness direction, under different superimposed hydrostatic pressures from 0 to 124 MPa.

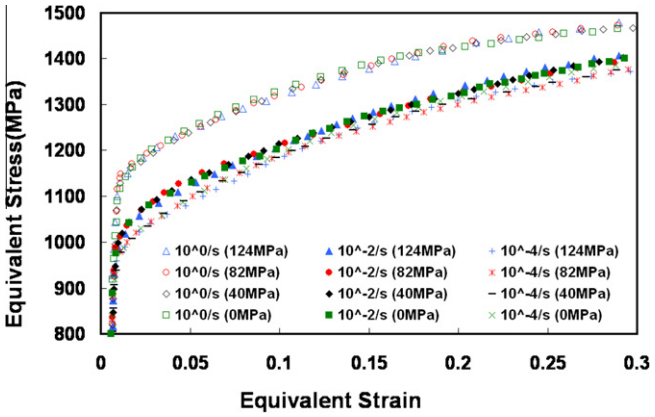

Fig. 14. Responses in compression along normal to rolling plane (ND), or through thickness direction, under different superimposed hydrostatic pressures ranging from 0 to 124 MPa, in terms of equivalent stresses and strains.

Table 1
The optimized material constants for KHL constitutive model.

Loading dir	A (MPa)	B (MPa)	n_0	n_1	C	m
RD	1273.12	868.44	0.5447	1.5343	0.0284	1.9368
TD	1106.01	754.45	0.5447	1.5343	0.0284	1.9368

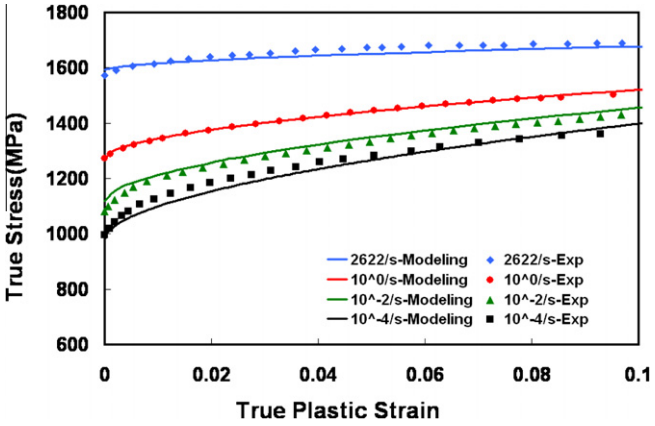

Fig. 15. The comparison between the experimental observation and numerical simulation along rolling direction at the temperature of 296 K and under various strain rates.

$$\sigma = \left[A + B\left(1 - \frac{\ln \dot{\varepsilon}}{\ln D_0^P}\right)^{n_1} \varepsilon^{n_0}\right]\left[\frac{\dot{\varepsilon}}{\dot{\varepsilon}^*}\right]^{C}\left[\frac{T_m - T}{T_{m-}T_r}\right]^{m}$$

where σ, ε and $\dot{\varepsilon}$ are the flow stress, the plastic strain and the current plastic strain rate, respectively. T, T_m and T_r are the current, melting and reference temperatures. $\dot{\varepsilon}^* = 1\ s^{-1}$ is the reference strain rate at which the strain rate effect term reduces to unity. $D_0^P = 10^6\ s^{-1}$ is a constant which is used to non-dimensionalize the strain rate term. In the KHL constitutive model, there are total six material constants: A, B, n_0, n_1, C, and m.

The six material constants in the KHL constitutive model are determined from the experimental observations by following the systematical method proposed by Khan and Liang (1999). Subsequently, these material constants determined from experimental data are imported into a least-squared based optimization program as initial values to obtain the final optimized material constants (Farrokh and Khan, 2009). The optimized material constants are listed in Table 1. It should be noted that only A and B constants, representing yield stress at a strain rate of $1\ s^{-1}$ and work hardening coefficient, respectively, are different for different anisotropy directions.

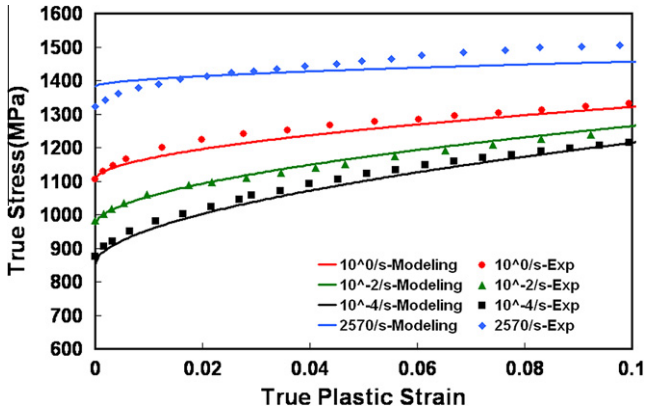

Fig. 16. The comparison between the experimental observation and numerical simulation along transverse-to-rolling direction at the temperature of 296 K and under various strain rates.

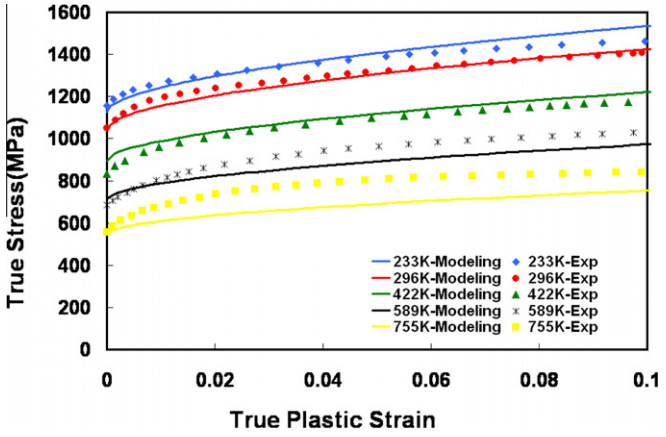

Fig. 17. The comparison between the experimental observation and numerical simulation along rolling direction at the strain rate of $10^{-3}\ s^{-1}$ and under various temperatures.

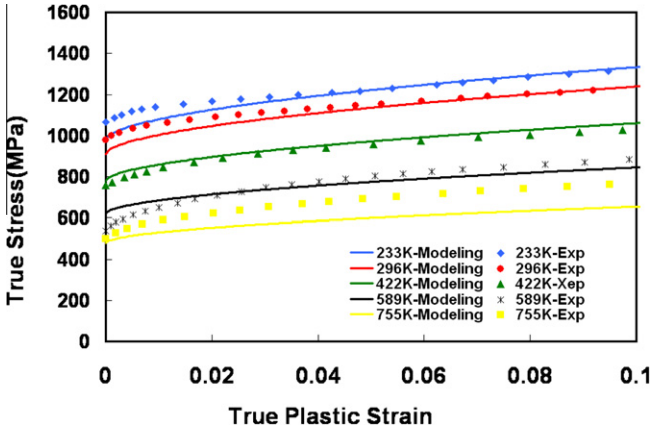

Fig. 18. The comparison between the experimental observation and numerical simulation along transverse-to-rolling direction at the strain rate of $10^{-3}\ s^{-1}$ and under various temperatures.

4.2. Correlations with the modified KHL constitutive model

The KHL phenomenological constitutive model is used to correlate the observed thermo mechanical responses of Ti–6Al–4V alloy at various strain rates and over a wide range of temperature, by using the material constants (listed in Table 1). The

numerical results of the KHL constitutive model at 296 K (reference temperature) and over a wide range of strain rates, from quasi-static to dynamic region, are compared with the corresponding experimental observations along rolling and transverse-to-rolling direction and are shown in Figs. 15 and 16, respectively. In these figures, it is clearly demonstrated that the correlations, for each loading direction, are in good agreement with the experimental observations at different strain rates.

In Figs. 17 and 18 are shown the experimental data along with the model correlations in rolling and transverse-to-rolling directions at the strain rate of 10^{-3} s^{-1}, and at different temperatures. It can be seen from these figures that, except for the highest temperature, the decrease of yield and flow stresses with the increase of temperature, or thermal softening effect, is successfully correlated for the both loading directions.

5. Summary

In this research, a systematic investigation was performed to explore the anisotropic thermo-mechanical behaviors of an electron beam single melt Ti–6Al–4V alloy, both experimentally and numerically, over a broad range of strain rates and temperatures. By comparing the true stress–true strain data obtained along the three principal material directions, it was found that the highest strength was achieved along the rolling direction, and similar mechanical responses were acquired along transverse-to-rolling and thickness directions. The experimental observation also showed that, along any principal material direction, the strength of the alloy, including yield stress, flow stress, as well as the work hardening rate, manifested an inverse dependency on the temperature, which was consistent with traditional thermal softening theories. Whereas, a positive strain rate effect on the strength was found through the examined strain rate range along all the loading directions. The mechanical responses of the alloy under different superimposed hydrostatic pressures and strain rates were also investigated. The stress–strain curves appeared to shift by the amount of applied superimposed hydrostatic pressures. However, the corresponding von Mises equivalent stress and strain curves manifested almost negligible sensitivity to the changing of hydrostatic pressure. It was also showed that the KHL constitutive model could be applied to capture the anisotropic mechanical responses of the alloy along different loading directions at broad ranges of strain rate and temperature.

References

Armstrong, R.W., Ramachandran, V., Zerilli, F.J., 1988. In: Rama Rao, P. (Ed.), Advances in Materials and Their Applications. Wiley Eastern Ltd., New Delhip, p. 201.

Bjerke, T., Li, Z., Lambros, J., 2002. Role of plasticity in heat generation during high rate deformation and fracture of polycarbonates. Int. J. Plast. 18 (4), 549–567.

Brownrigg, A., Spitzig, W.A., Richmond, O., Teirlinck, D., Embury, J.D., 1983. The influence of hydrostatic pressure on the flow stress and ductility of a spherodized 1045 steel. Acta Metall. 31 (8), 1141–1150.

Cheng, J., Nemat-Nasser, S., 2000. A model for experimentally-observed high-strain-rate dynamic strain aging in titanium. Acta Mater. 48 (12), 3131–3144.

Chichili, D.R., Ramesh, K.T., Hemker, K.J., 1998. The high strain rate response of alpha-titanium: experiments, deformation mechanisms and modeling. Acta Meter. 46 (3), 1025–1043.

Conrad, H.M., Doner, M., De Meester, B., 1973. Critical review deformation and fracture. In: International Conference on Titanium, Proceedings of Titanium Science and Technology. Massachusetts Institute of Technology, Boston, p. 969.

Farrokh, B., Khan, A.S., 2009. Grain size, strain rate, and temperature dependence of flow stress in ultra-fine grained and nanocrystalline Cu and Al: synthesis, experiment, and constitutive modeling. Int. J. Plast. 25 (5), 715–732.

Follansbee, P.S., Gray III, G.T., 1989. An analysis of the low temperature, low and high strain-rate deformation of Ti–6Al–4V. Metall. Trans. A 20 (5), 863–874.

Gilat, A., Cheng, C.S., 2002. Modeling torsional split Hopkinson bar tests at strain rates above 10,000 per sec. Int. J. Plast. 18 (5–6), 787–799.

Hoge, K., Mukhejee, K., 1977. The temperature and strain rate dependence of the flow stress of tantalum. J. Mater. Sci. 12, 1666–1672.

Huang, S., Khan, A.S., 1991. On the use of electrical-resistance metallic foil strain gages for measuring large dynamic plastic deformation. Exp. Mech. 31, 122–125.

Johnson, G.R., Cook, W.H., 1983. A constitutive model and data for metals subjected to large strains, high strain rates and high temperatures. In: Proceedings of the Seventh International Symposium on Ballistic, The Hague, The Netherlands, 1983, p. 541.

Kao, A.S., Kuhn, H.A., Richmond, O., Spitzig, W.A., 1989. Workability of 1045 spheroidized steel under superimposed hydrostatic pressure. Metall. Trans. A 20A, 1735–1741.

Khan, A.S., Baig, M., 2011. Anisotropic responses, constitutive modeling and the effects of strain-rate and temperature on the formability of an aluminum alloy. Int. J. Plast. 27, 522–538.

Khan, A.S., Baig, M., Choi, S., Yang, H., Sun, X., 2012. Quasi-static and dynamic responses of advanced high strength steels: experiments and modeling. Int. J. Plast. 30–31, 1–17.

Khan, A.S., Kazmi, R., Farrokh, B., et al, 2007a. Effect of oxygen content and microstructure on the thermo-mechanical response of three Ti–6Al–4V alloys: experiments and modeling over a wide range of strain-rates and temperatures. Int. J. Plast. 23, 1105–1125.

Khan, A.S., Liang, R., 1999. Behaviors of three BCC metal over a wide range of strain rates and temperatures: experiments and modeling. Int. J. Plast. 15 (9), 1089–1109.

Khan, A.S., Suh, Y.S., Kazmi, R., 2004. Quasi-static and dynamic loading responses and constitutive modeling of titanium alloys. Int. J. Plast. 20, 2233–2248.

Khan, A.S., Zhang, H., 2000. Mechanically alloyed nanocrystalline iron and copper mixture: behavior and constitutive modeling over a wide range of strain rates. Int. J. Plast. 16 (12), 1477–1492.

Lesuer, D.R. 2000. Experimental investigations of material models for Ti–6Al–4V titanium and 2024–T3 aluminum. In: Final Report, DOT/FAA/AR-00/25, US Department of Transportation, Federal Aviation Administration.

Macdougall, D.A.S., Harding, J., 1999. A constitutive relation and failure criterion for Ti–6Al–4V alloy at impact rates of strain. J. Mech. Phys. Solids 47 (5), 1157–1185.

Majorell, A., Srivatsa, S., Picu, R.C., 2002. Mechanical behavior of Ti–6Al–4V at high and moderate temperatures – Part I: experimental results. Mater. Sci. Eng., A 326 (2), 297–305.

Mecking, H., Kocks, U.F., 1981. Kinetics of flow and strain-hardening. Acta Metall. 29, 1865–1875.

Meyers, M.A., Subhash, G., Kad, B.K., Prasad, L., 1994. Evolution of microstructure and shear-band formation in A-hcp titanium. Mech. Mater. 17 (2–3), 175–193.

Molinari, A., Musquar, C., Sutter, G., 2002. Adiabatic shear banding in high speed machining of Ti–6Al–4V: experiments and modeling. Int. J. Plast. 18 (4), 443–459.
Montgomery, J.S., Wells, M.G.H., 2001. Titanium armor applications in combat vehicles. JOM 53 (4), 29–32.
Nemat-Nasser, S., Guo, W., Nesterenko, V.F., Indrakanti, S.S., Gu, Y., 2001. Dynamic response of conventional and hot isostatically pressed Ti–6Al–4V alloys: experiments and modeling. Mech. Mater. 33 (8), 425–439.
Nemat-Nasser, S., Li, Y., 1998. Flow stress of F.C.C. polycrystals with application to OFHC Cu. Acta Mater. 46 (2), 565–577.
Nemat-Nasser, S., Tomoo, O., Ni, L., 1998. A physically-based constitutive model for BCC crystals with application to polycrystalline tantalum. J. Mech. Phys. Solids. 46 (6), 1009–1038.
Nixon, M.E., Cazacu, O., Lebensohn, R.A., 2010. Anisotropic response of high-purity a-titanium: Experimental characterization and constitutive modeling. Int. J. Plast. 26 (2010), 516–532.
Peirce, D., Asaro, R.J., Needleman, A., 1983. Material rate dependence and localized deformation in crystalline solids. Acta Metall. 31, 1951–1976.
Rosakis, P., Rosakis, A.J., Ravichandran, G., Hodowany, J., 2000. A thermodynamic internal variable model for the partition of plastic work into heat and stored energy in metals. J. Mech. Phys. Solids 48 (3), 581–607.
Song, S.G., Gray III, G.T., 1995. Structural interpretation of the nucleation and growth of deformation twins in Zr and Ti – I. Application of the coincidence site lattice (CSL) theory to twinning problems in H.C.P. structures. Acta Metall. Mater. 43 (6), 2325–2337.
Spitzig, W.A., Richmond, O., 1984. The effect of pressure on the flow stress of metals. Acta Metall. 32 (3), 457–463.
Steglich, D., Brocks, W., Bohlen, J., Barlat, F., 2011. Modeling direction-dependent hardening in magnesium sheet forming simulations. Int. J. Mater. Form. 4, 243–253.
Sung, J.H., Kim, J.H., Wagoner, R.H., 2010. A plastic constitutive equation incorporating strain, strain-rate, and temperature. Int. J. Plast 26, 1746–1771.
Zerilli, F.J., Armstrong, R.W., 1987. Dislocation-mechanics-based constitutive relations for material dynamics calculations. J. Appl. Phys. 61 (5), 1816–1825.